JACS
JOURNAL OF THE AMERICAN CHEMICAL SOCIETY
Article
pubs.acs.org/JACS

Highly Active Au/δ-MoC and Cu/δ-MoC Catalysts for the Conversion of CO_2: The Metal/C Ratio as a Key Factor Defining Activity, Selectivity, and Stability

Sergio Posada-Pérez,[†] Pedro J. Ramírez,[‡] Jaime Evans,[‡] Francesc Viñes,[†] Ping Liu,[§] Francesc Illas,*[,†] and José A. Rodriguez*[,§]

[†]Departament de Química Física and Institut de Química Teòrica i Computacional (IQTCUB), Universitat de Barcelona, c/Martí i Franquès 1, 08028 Barcelona, Spain

[‡]Facultad de Ciencias, Universidad Central de Venezuela, Caracas 1020-A, Venezuela

[§]Chemistry Department, Brookhaven National Laboratory, Upton, New York 11973, United States

Supporting Information

ABSTRACT: The ever growing increase of CO_2 concentration in the atmosphere is one of the main causes of global warming. Thus, CO_2 activation and conversion toward valuable added compounds is a major scientific challenge. A new set of Au/δ-MoC and Cu/δ-MoC catalysts exhibits high activity, selectivity, and stability for the reduction of CO_2 to CO with some subsequent selective hydrogenation toward methanol. Sophisticated experiments under controlled conditions and calculations based on density functional theory have been used to study the unique behavior of these systems. A detailed comparison of the behavior of Au/β-Mo_2C and Au/δ-MoC catalysts provides evidence of the impact of the metal/carbon ratio in the carbide on the performance of the catalysts. The present results show that this ratio governs the chemical behavior of the carbide and the properties of the admetal, up to the point of being able to switch the rate and mechanism of the process for CO_2 conversion. A control of the metal/carbon ratio paves the road for an efficient reutilization of this environmental harmful greenhouse gas.

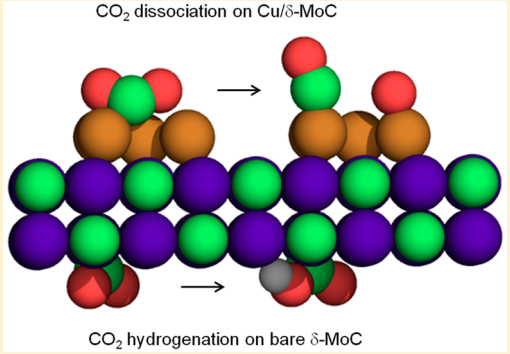

INTRODUCTION

It is nowadays well-accepted that the vast and exceeding emissions derived from human activities related to fossil fuels[1] have led to an excessive concentration of carbon dioxide (CO_2) in the atmosphere with concomitant problems in the environment.[2] Consequently, to mitigate the resulting harmful effects, CO_2 capture, storage, and, especially, its conversion to valuable fuels and precursors have become an urgent need. Many studies have been carried out in order to provide an effective capture and sequestration of CO_2, although it seems clear that the efforts must be routed toward the potential use of CO_2 as an economical feedstock.[3,4] Within the framework of CO_2 conversion,[5] several routes for CO_2 reduction toward carbon monoxide (CO), methanol (CH_3OH), and hydrocarbons are possible. In this respect, CO_2 reduction to CO has become an interesting option since the CO thus produced could be used as feedstock in the Fischer−Tropsch synthesis of fuels or as the starting point for the production of chemicals or commodity goods in the industry.[5−8] Since a fraction of the CO_2 in the atmosphere could be used to cover the industrial needs of methanol,[5] direct hydrogenation of CO_2 to this alcohol ($CO_2 + 3H_2 \rightarrow CH_3OH + H_2O$) is drawing a lot of attention.[5,9−11]

Clearly the design of new cost-effective catalysts able to produce CO and CH_3OH from CO_2 is a chief challenge.[5] In the current search for new catalysts,[12] transition-metal carbides (TMCs) are appealing as an alternative to precious (and expensive) metals for many reactions[13−23] due to their abundance, relatively low cost, and, apparently, smaller activation energy barriers for reactions such as for O−O bond cleavage.[24] Some TMCs bind CO_2 well and can induce the cleavage of C−O bonds by themselves or assisted by hydrogen.[17,25−28] Thus, they have activity for the conversion of CO_2. Furthermore, TMCs behave as excellent supports for the dispersion and activation of small metal particles.[29] The latter comes from their capability to modify the electronic structure of the supported metal particles with a concomitant increase in the catalytic activity.[28−31] Nevertheless, a problem associated with the use of TMCs as catalysts is their tendency to form oxycarbides when exposed to oxygen-containing molecules,[8,25,32] so in the search for a viable catalyst for CO_2 conversion, this trend must be minimized.

A recent theoretical study has examined the bonding of CO_2 with ZrC, TaC, NbC, HfC, TiC, and δ-MoC substrates.[27]

Received: May 2, 2016
Published: June 16, 2016

DOI: 10.1021/jacs.6b04529
J. Am. Chem. Soc. 2016, 138, 8269−8278

Among these carbides, δ-MoC exhibits a promising behavior for activating CO_2.[17,27] In this paper, we report a combined experimental and theoretical study of CO and CH_3OH production from CO_2 hydrogenation on catalysts based on the Au/δ-MoC and Cu/δ-MoC systems. These catalysts are able to produce CO and a noteworthy amount of methanol avoiding methane production as well as precluding catalyst deactivation due to oxycarbide formation. By comparing to the behavior seen for Au/Mo_2C and Cu/Mo_2C, it is argued that the metal/carbon ratio in the carbide is crucial to control interactions with the supported Au or Cu nanoparticles and the overall performance (activity, selectivity and stability) of the catalysts for CO_2 conversion.

EXPERIMENTAL DETAILS

We investigated the performance for the hydrogenation of CO_2 of a series of catalysts generated by the deposition of Au and Cu on TiC(001), polycrystalline δ-MoC, and β-Mo_2C(001) surfaces. The experimental data were collected in a setup that combined an ultrahigh vacuum (UHV) chamber for surface characterization and a microreactor for catalytic tests.[17,33] The UHV chamber was equipped with instrumentation for X-ray photoelectron spectroscopy (XPS), low-energy electron diffraction (LEED), ion-scattering spectroscopy (ISS), and thermal-desorption mass spectroscopy (TDS).[33]

The TiC(001) and β-Mo_2C(001) surfaces were prepared and cleaned as described in previous works.[33] The δ-MoC examined in this study is best described as polycrystalline.[34] Surface impurities were removed by Ar^+ sputtering, and a C/Mo ratio close to 1 was restored by exposing this surface to C_2H_2 or C_2H_4 at 800−900 K.[34] Several attempts were made to prepare well-defined surfaces of δ-MoC oriented along the (001) plane of this carbide. However, it was not possible to prepare an ideal δ-MoC(001) surface. The preparation of this particular surface is very difficult due to the complex phase diagram of MoC.[35] Au and Cu were vapor deposited on the metal carbide substrates at 300 K.[23,26,28]

In the studies of CO_2 hydrogenation, the sample was transferred to the reactor at ∼300 K, then the reactant gases, 0.049 MPa (0.5 atm) of CO_2 and 0.441 MPa (4.5 atm) of H_2, were introduced and the sample was rapidly heated to the reaction temperature (500, 525, 550, 575, and 600 K). Product yields were analyzed by a gas chromatograph.[36,37] In our experiments, data were collected at intervals of 15 min. The amount of molecules (CO, CH_4, or CH_3OH) produced in the catalytic tests was normalized by the active area exposed by the sample and the total reaction time. The kinetic experiments were done in the limit of low conversion (<5%).

COMPUTATIONAL MODELS AND METHODS

The experiments described in detail in the forthcoming sections indicated that the best catalyst found in this work for the hydrogenation of CO_2 was Cu/δ-MoC. Therefore, theoretical efforts were addressed to model this particular type of catalyst, and this was, in turn, achieved by considering the Cu/δ-MoC(001) system.[38] In a first step, the (001) surface of cubic δ-MoC was chosen since it is the most stable and so likely to be most exposed one.[39] This surface was represented by periodic slab models containing four atomic layers, and in a second step, a Cu_4 cluster model was supported as in previous work.[38] The reactivity of both, bare δ-MoC(001) and Cu_4/δ-MoC(001), catalyst models toward CO_2 reduction and hydrogenation was considered. In the corresponding calculations, the two outermost layers were relaxed and the two bottommost fixed. For the clean surface, previous studies showed that using thicker slabs leads to structural and energetic properties variations below 5%.[39] In all models, a vacuum region with a width larger than 10 Å is added in the direction perpendicular to the surface.

The density functional theory (DFT)-based calculations employed the Perdew−Burke−Erzerhof (PBE) functional[40] and were carried out using the Vienna Ab initio Simulation Package (VASP).[41] The valence electron density is expanded in a plane-wave basis set with a cutoff of 415 eV for the kinetic energy, and the effect caused by the core electrons on the valence region is described by the projector augmented wave method of Blöchl,[42] as implemented by Kresse and Joubert.[43] A 3 × 3 × 1 grid of special *k*-point within the Monkhorst−Pack[44] scheme was used for the necessary integration steps in the reciprocal space. The threshold for electronic relaxation was $<10^{-5}$ eV, and relaxation of the atomic positions was allowed until forces acting on the atoms are always smaller than 0.01 eV $Å^{-1}$. Transition-state structures have been located using the DIMER method[45] and fully characterized via pertinent frequency analysis of the modes related to the adsorbate within the harmonic approximation. Hence, vibrational frequencies obtained from the diagonalization of the pertinent block of the Hessian matrix whose elements are computed as finite differences of analytical gradients. All adsorption energy values and energy barriers have been corrected to account for the zero point energy within the harmonic approximation.

In order to provide better comparison to experiment, the Gibbs free energy (G) profile for the reaction pathways of interest have also been obtained, thus allowing taking into account temperature and pressure effects. The Gibbs free energy has been calculated following the approximate procedure proposed by Nørskov et al.[46] summarized in eq 1 below

$$\Delta G_A = \Delta H_A - T(S_A - S_R) \quad (1)$$

where the ΔG_A is the free energy of a step A, ΔH_A is the enthalpy change associated with the step A and, in absence of mechanical work, approximated by the corresponding change in total energy, T is the absolute temperature, and S_A and S_R are the entropy of the products and reactants for step A. In practice, the entropy of gas-phase species is computed by taking into account all contributions to the partition function with the assumption of rigid rotor and harmonic frequencies, whereas it is customary to neglect the entropy of adsorbed species. This implies the main changes in going from the total energy to Gibbs free energy profiles involves adsorption and desorption steps. In this paper the free energy profiles have been carried out taking into account the entropy of all gas-phase species. For the adsorbed species, the entropy (S_{ν_i}) contributions have been calculated as in eq 2, while neglecting the remaining (rotation and translation) degrees of freedom:

$$S_{\nu_i} = -k_B \ln(1 - e^{-\hbar\nu_i/(k_B T)}) \quad (2)$$

where ν_i corresponds to the harmonic vibrational frequency of the i^{th} vibrational degree of freedom, and k_B and $\hbar$ are the Boltzmann and Planck constants, respectively. To compute the zero point energy and the corresponding contribution to entropy, all calculated frequencies have been taken into account. Nevertheless, note that, as pointed out by Nørskov et al.,[46] only frequencies smaller than 50 cm^{-1} significantly affect the entropy contribution to the Gibbs free energy.

RESULTS AND DISCUSSION

Experiments. Figure 1 collects data for the hydrogenation of CO_2 on the bare TiC(001), δ-MoC, and orthorhombic β-Mo_2C(001) surfaces.[17,28] On the TMCs with a metal/carbon ratio of 1, left-side panel in Figure 1, we detected only the production of CO and methanol. In contrast, on a metal carbide with a metal/carbon ratio of 2, β-Mo_2C(001) in the right-side panel of Figure 1, there was production of a large amount of methane in addition to CO and methanol. This difference in selectivity reflects variations in the bonding modes of CO_2 on the different carbides.[17,27,28] In general, a decrease in the metal/carbon ratio in a carbide usually reduces the reactivity of the system as a consequence of electronic, a raise in the positive charge on the metal centers, and structural effects, a reduction in the number of metal centers exposed on the carbide surface.[47,48] Theoretical calculations indicate that CO_2 adsorbs molecularly on TiC(001) and δ-MoC(001).[17,27,28]

DOI: 10.1021/jacs.6b04529
J. Am. Chem. Soc. 2016, 138, 8269−8278

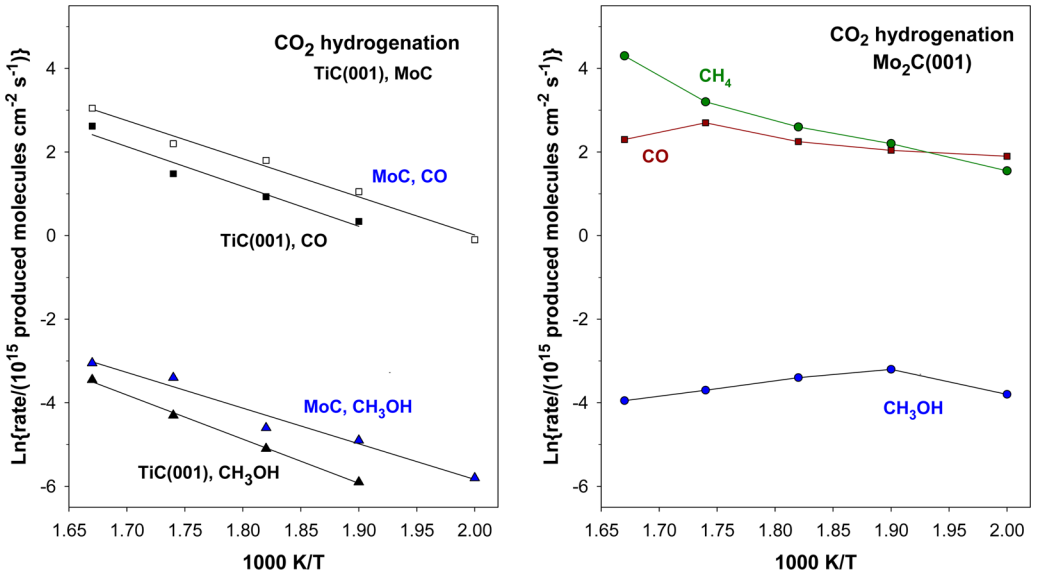

Figure 1. Hydrogenation of CO_2 on TiC(001), polycrystalline δ-MoC, and orthorhombic β-Mo_2C(001). Arrhenius plots for the production of CO, methanol, and methane (only seen on the β-Mo_2C(001) catalyst). In a batch reactor, the catalysts were exposed to 0.049 MPa (0.5 atm) of CO_2 and 0.441 MPa (4.5 atm) of H_2 at temperatures of 600, 575, 550, 525, and 500 K.

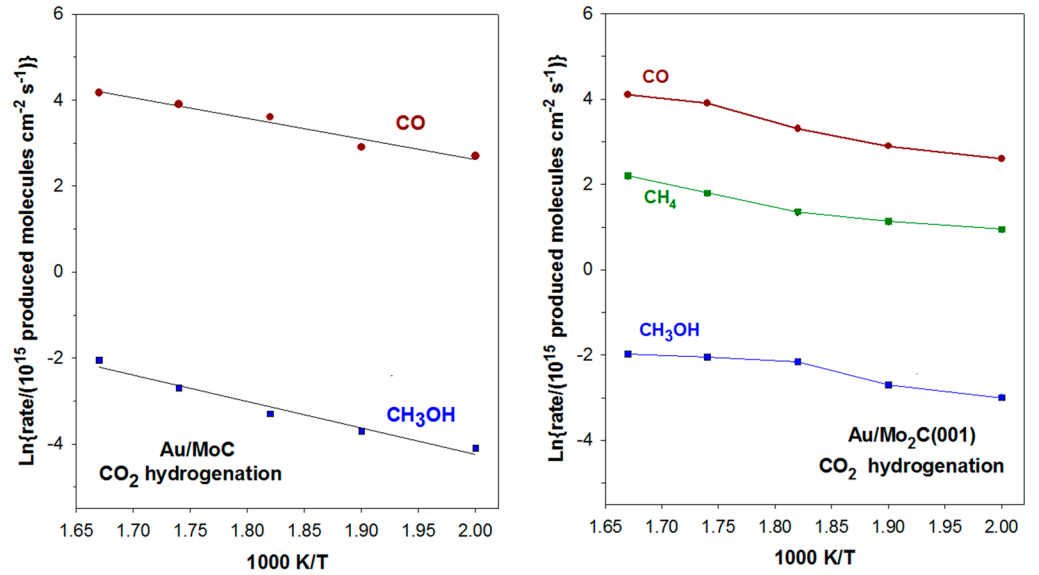

Figure 2. Hydrogenation of CO_2 on Au/δ-MoC and Au/β-Mo_2C(001) surfaces. Arrhenius plots for the production of CO, methanol, and methane (only seen on the β-Mo_2C(001) catalyst). In a batch reactor, the catalysts were exposed to 0.049 MPa (0.5 atm) of CO_2 and 0.441 MPa (4.5 atm) of H_2 at temperatures of 600, 575, 550, 525, and 500 K.

The cleavage of a C−O bond occurs only after hydrogenation of the molecule and formation of a COOH intermediate.[28] On the other hand, one of the C−O bonds in carbon dioxide dissociates rather easily on β-Mo_2C(001), and dissociation of the second requires only a relatively small activation barrier.[17,26,49] The C deposited on this carbide is hydrogenated to produce methane.[17,26]

The catalytic performance of metal carbides can be enhanced by adding transition or noble metals to their surfaces.[5,23,28−31] Au and Cu adatoms undergo electronic perturbations when in contact with TMC(001) surfaces.[29] Results of scanning tunneling microscopy (STM) indicate that at small coverages (θ < 0.2 ML), Au and Cu grow on TiC(001) forming very small particles, many of them two-dimensional.[50−52] Although bulk metallic gold is not catalytically active, small particles of this element in contact with TiC(001) display an extraordinary activity for desulfurization reactions,[51] CO oxidation,[53] and the water−gas shift reaction.[54] On the basis of these previous studies, we tested the CO_2 hydrogenation ability of catalysts generated by depositing Au and Cu on the carbide surfaces shown in Figure 1.

Figure 2 displays Arrhenius plots for the rates of CO, CH_3OH, and CH_4 production on Au/δ-MoC and Au/β-Mo_2C(001) surfaces with a gold coverage close to 0.2 ML. Extended surfaces of Au do not catalyze the reduction of CO_2 or the synthesis of methanol from CO_2 hydrogenation. In contrast, small gold aggregates dispersed on the carbide surfaces are active for these chemical reactions. On δ-MoC, the addition of gold enhances the rates of formation of CO and CH_3OH by a factor of 3. The enhancement of these rates of

DOI: 10.1021/jacs.6b04529
J. Am. Chem. Soc. 2016, 138, 8269−8278

formation is large on β-$Mo_2C(001)$ because gold substantially reduces the formation of methane on this carbide surface (Figure 3). The gold atoms probably nucleate on the sites of

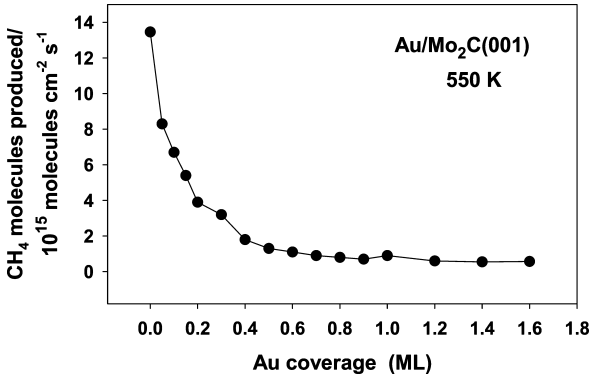

Figure 3. Rate of methane production on a fresh Au/β-$Mo_2C(001)$ catalyst as a function of gold coverage. In a batch reactor, the catalysts were exposed to 0.049 MPa (0.5 atm) of CO_2 and 0.441 MPa (4.5 atm) of H_2 at a temperature of 550 K.

the β-$Mo_2C(001)$ substrate that are highly active for the complete dissociation of CO_2. In Figure 2, the rates of CO formation on Au/MoC and Au/β-$Mo_2C(001)$ are comparable, but on the system in which the carbide has a metal/carbon ratio of 1, there is no methane formation. This increase in selectivity was accompanied by an increase in stability (Figure 4). After

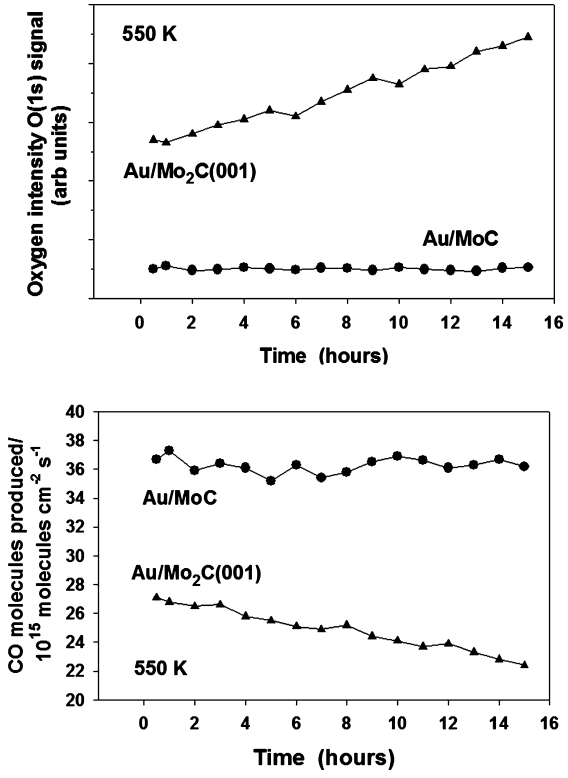

Figure 4. Top: Variation of the oxygen intensity in O 1s XPS spectra for Au/δ-MoC and Au/β-$Mo_2C(001)$ catalysts ($\theta_{Au} \sim 0.2$ ML) as a function of time. Bottom: Rate of CO production for the Au/δ-MoC and Au/β-$Mo_2C(001)$ catalysts as a function of time. In a batch reactor, the catalysts were exposed to 0.049 MPa (0.5 atm) of CO_2 and 0.441 MPa (4.5 atm) of H_2 at a temperature of 550 K.

reaction, XPS showed the presence of a minor amount of oxygen (~0.1 ML) on the MoC substrate. This oxygen coverage did not increase with time inducing a drop in catalytic activity (Figure 4). A very different behavior was found for Au/β-$Mo_2C(001)$. The amount of oxygen present on this carbide system after reaction was large (>0.4 ML) and increased with time (Figure 4), probably due to the formation of an oxycarbide. As result of this, the Au/β-$Mo_2C(001)$ system exhibited poor stability since the surface activity decreased due to the O poisoning (Figure 4). These results show that the metal/carbon ratio in the TMC is critical if one is aiming for a catalyst with good activity, selectivity, and stability for the reduction of CO_2 to CO. In the rest of the article, we will focus our attention on carbide catalysts containing a 1:1 metal/carbon ratio: δ-MoC and TiC.

Figure 5 shows the effects of Au and Cu coverage on the activity for CO production of δ-MoC and TiC(001) systems.

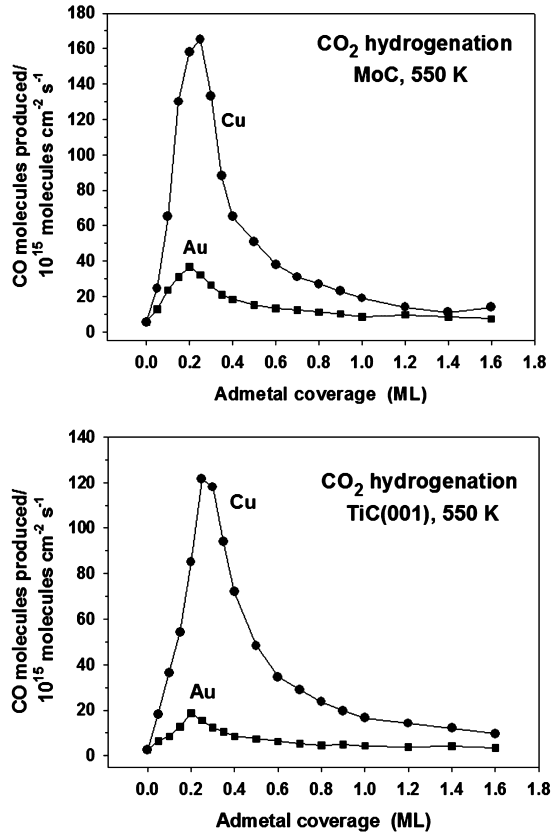

Figure 5. Rate of CO production on δ-MoC, top, and TiC(001), bottom, for different coverages of Au and Cu. In a batch reactor, the catalysts were exposed to 0.049 MPa (0.5 atm) of CO_2 and 0.441 MPa (4.5 atm) of H_2 at a temperature of 550 K.

On both carbide surfaces, the deposition of Cu produces the best catalysts. A maximum of catalytic activity is seen at admetal coverages of 0.2−0.25 ML. An identical result was obtained after plotting the rate for the production of methanol instead of the rate for the production of CO. One can correlate the results obtained for Cu/TiC(001) and Au/TiC(001) with particle size distributions found in STM.[50−52] The largest rate of CO (or methanol) production per admetal atom was seen at coverages below 0.2 ML when many of the admetal particles are very small (<1 nm) and two-dimensional.[50−52] The same is probably valid for the Cu/MoC and Au/MoC systems. Once the

DOI: 10.1021/jacs.6b04529
J. Am. Chem. Soc. 2016, 138, 8269−8278

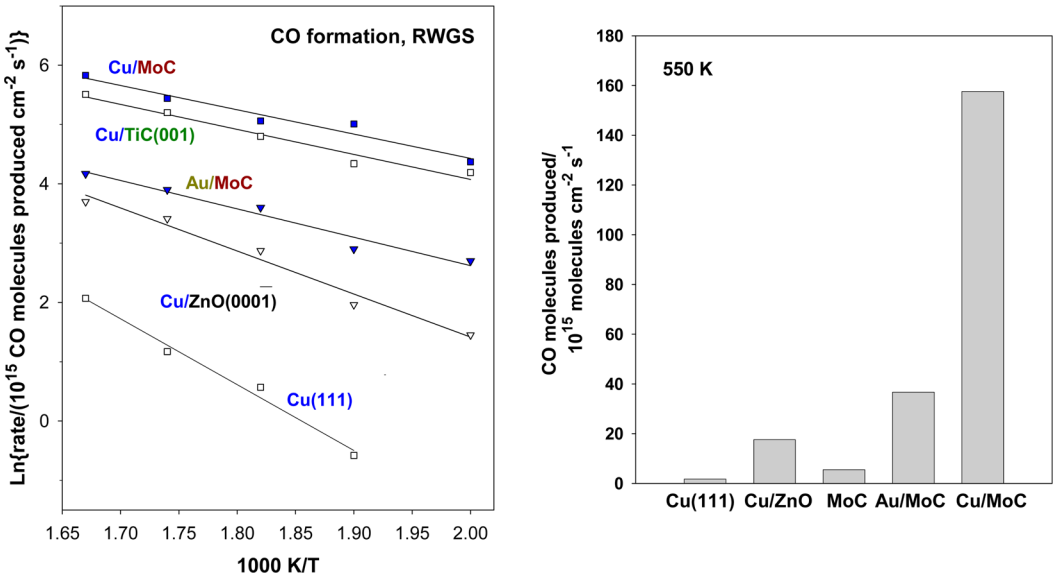

Figure 6. Left: Arrhenius plots for the production of CO by CO_2 hydrogenation on a series of gold- and copper-containing catalysts. The Cu and Au coverages on δ-MoC and TiC(001) were close to 0.2 ML. In a batch reactor, the catalysts were exposed to 0.049 MPa (0.5 atm) of CO_2 and 0.441 MPa (4.5 atm) of H_2 at temperatures of 600, 575, 550, 525, and 500 K. Right: Comparison of the rates for CO production at 550 K.

particles become larger (>2 nm), the chemical and catalytic activity decreases. In the case of very small Au or Cu particles, the effects of the Au-carbide or Cu-carbide interface are very significant, and most of the admetal atoms could work in a cooperative way with atoms of the carbide substrate.

Figure 6 shows Arrhenius plots for the production of CO on a series of Cu- and Au-based catalysts. The derived apparent activation energies are listed in Table 1. From the slopes of the lines in Figures 6, it is clear that the Cu/δ-MoC system has a lower apparent activation energy, 9 kcal/mol, than clean δ-MoC, 18 kcal/mol, or plain Cu(111),[37] 22 kcal/mol. From the data in Figure 6, one can conclude that the Cu/δ-MoC system has unique properties for the reduction of CO_2 into CO. The bare δ-MoC material presents worse activity than a model of a commercial Cu/ZnO catalysts,[37] but upon the addition of a small amount of Cu, one obtains a remarkable catalyst for the reduction of CO_2. In fact, Au/δ-MoC also exhibits a better activity than Cu/ZnO, although its performance is not as good as that of Cu/δ-MoC.

Table 1. Apparent Activation Energies (in kcal/mol)[a]

catalyst	CO, RWGS	CH_3OH synthesis
Cu/δ-MoC	9 (0.39)	10 (0.43)
Cu/TiC(001)	9 (0.39)	11 (0.48)
Au/ δ-MoC	10 (0.43)	12 (0.52)
Au/TiC(001)	14 (0.61)	13 (0.57)
δ-MoC	18 (0.78)	17 (0.74)
TiC(001)	19 (0.35)	21 (0.91)
Cu/ZnO(000$\bar{1}$)[b]	14 (0.61)	16 (0.69)
Cu(111)[b]	22 (0.95)	25 (1.08)

[a]For comparison, eV values are given in parentheses. [b]From ref 37.

In the metal/carbide catalysts in Figure 6, the rate for CO formation was 10^2–10^3 times faster than the rate for methanol synthesis. Nevertheless, all these catalysts displayed an activity for methanol synthesis which was much larger than that of Au(111), Cu(111), or a Cu/ZnO catalyst (Figure 7). In this aspect, Cu/δ-MoC is clearly the best catalyst among the catalysts studied. The apparent activation energy decreases from 25 kcal/mol on Cu(111)[37] to 16 kcal/mol on Cu/ZnO(000$\bar{1}$)[37] and to only 10 kcal/mol on Cu/δ-MoC. This surface has a catalytic activity that is 8–11 times higher than that of Cu/ZnO(000$\bar{1}$),[37] illustrating the advantage in using a carbide as a metal support. Since catalytic activity of Cu/δ-MoC is much larger than that of Cu(111) or δ-MoC, it is likely that there is a synergy in the copper-carbide interface that favors the adsorption and transformation of CO_2. A similar phenomenon is probably occurring in the gold-carbide interface.

In Table 1, the apparent activation energies for CH_3OH and CO formation on a given surface have similar values suggesting that CO formation constitutes the rate-limiting step in all the metal/carbide systems. Accordingly, CO is likely to be formed first, and a fraction of it further converted into CH_3OH through selective hydrogenation steps.

Computational Study. To better understand the chemistry involved in the experiments described above for Cu/MoC-based catalysts, DFT-based calculations have been carried out on a series of systems using δ-MoC(001) and Cu_4/δ-MoC(001) as appropriate models of the catalysts using in experiments. As already commented, the choice for the δ-MoC (001) surface comes from the fact that it constitutes the most stable surface,[39] and consequently, it is likely to be the most exposed surface in the experimental polycrystalline catalysts.

In a previous work, DFT studies showed that on clean δ-MoC (001), the CO_2 molecules adsorbs through the C atom on above the three-fold hollow site formed by two Mo and one C atoms. In this adsorption mode, the CO_2 molecule is activated and C═O bonds are elongated,[17] a feature also exhibited by other TMCs.[27] Nevertheless, CO_2 direct dissociation is not favored since it involves a large energy barrier of 1.41 eV. A large energy barrier is also found for CO_2 dissociation on a TiC(001) substrate.[33] On the other hand, CO_2 dissociates almost spontaneously into CO on a β-Mo_2C(001) surface.[17,26] As mentioned above, a decrease in the metal/carbon ratio when going from β-Mo_2C(001) to δ-MoC(001) reduces the reactivity of the surface due to an increase in the positive charge on the Mo centers and structural

DOI: 10.1021/jacs.6b04529
J. Am. Chem. Soc. 2016, 138, 8269–8278

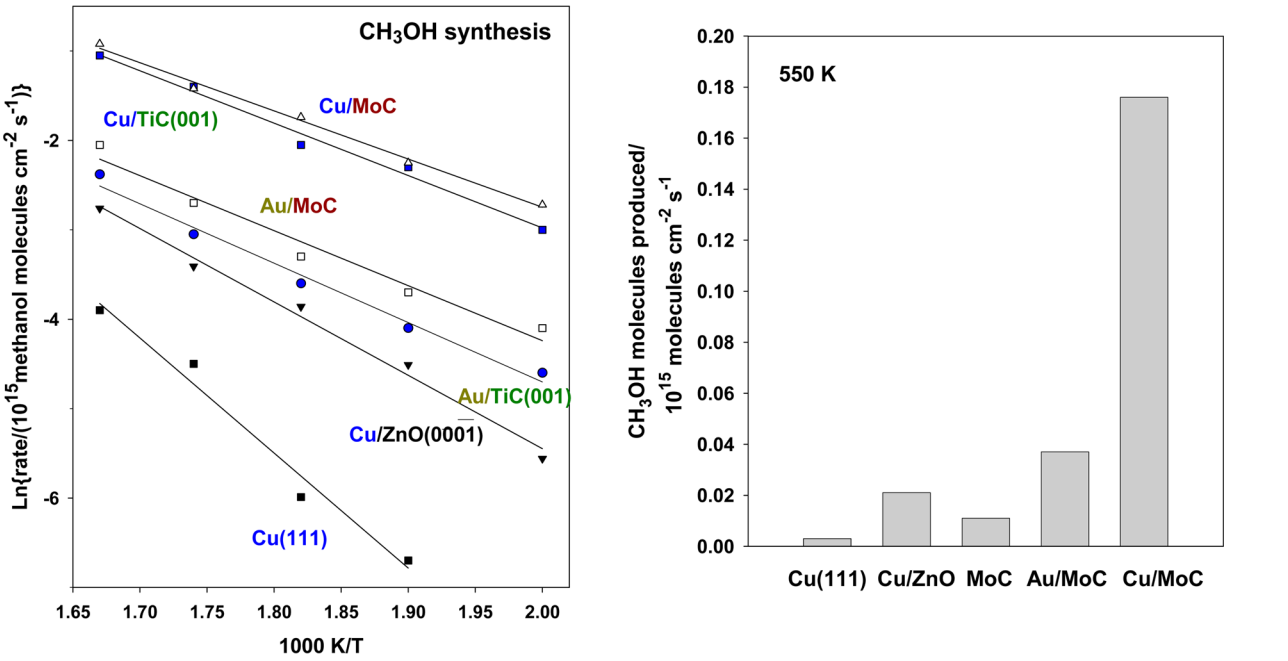

Figure 7. Left: Arrhenius plots for the production of methanol by CO_2 hydrogenation on a series of gold- and copper-containing catalysts. The Cu and Au coverages on MoC and TiC(001) were close to 0.2 ML. In a batch reactor, the catalysts were exposed to 0.049 MPa (0.5 atm) of CO_2 and 0.441 MPa (4.5 atm) of H_2 at temperatures of 600, 575, 550, 525, and 500 K. Right: Comparison of the rates for methanol production at 550 K.

changes that lower the number of exposed Mo atoms.[17,47,48] The reduction in the reactivity toward CO_2 is accompanied by a reduction in the binding energy of O adatoms[17] which is crucial for avoiding deactivation by the formation of an oxycarbide on the catalyst surface. Thus, the metal/carbon ratio plays a key role for defining the activity, selectivity, and stability of δ-MoC(001) as a catalytic material.

The energy profile in Figure 8a explores various particular elementary steps of interest for the full reaction map of CO_2 hydrogenation on bare δ-MoC(001) and aims at providing the main trends of the underlying molecular mechanism. Figure 8a shows that CO can be generated through initial CO_2 hydrogenation to COOH, entailing an energy barrier of 0.78 eV only, i.e. ∼ 0.6 eV lower than direct dissociation. In principle, direct hydrogenation of CO_2 to formate (HCOO) could also occur, but this involves a much higher energy barrier (1.76 eV), and hence, this route has not been further considered. The COOH species can evolve to CO through a barrier of 0.31 eV. Calculations also show that CO hydrogenation toward CH_3OH via HCO is more favorable than the route involving COH due to the endothermic character of the elementary step leading to the COH intermediate presenting a reaction energy very similar to the energy barrier for HCO formation. Besides, the predominance of HCO route is in agreement with previous studies on β-Mo_2C[22,26,55] and on metal surfaces.[56,57] The experimental observations displayed in Figures 6 and 7 are consistent with this picture since the apparent energy barriers for CO_2 hydrogenation to CO and CH_3OH in Table 1 are similar and, even if rigorously speaking a direct comparison is not possible, close to those predicted from the theoretical calculations. Also, the present model calculations are consistent with the observed CO:CH_3OH selectivity since dehydrogenation of some intermediates is favorable with respect to the methanol synthesis, including the desorption process. Moreover, that methane production is not detected in the experiments is also consistent with the difficulty of δ-MoC(001) to dissociate CO which implies a barrier of 1.79 eV. The fact that CH_4 is not observed implies that other possible routes involving, for instance, CO dissociation assisted by H would also exhibit rather high activation energy barriers. Regarding the comparison between calculated activation energy barriers and the measured apparent activation energy, one must point out that, for surface reactions involving several elementary steps, this is far from being straightforward and usually requires sophisticated simulations based on microkinetic[58] or kinetic Monte Carlo[59] algorithms. Nevertheless, it is worth pointing out that kinetic experimental data and the theoretical energy barriers show similar trends. In the particular case of CO_2 hydrogenation to methanol, both experiment and computational models are in qualitative agreement, indicating that it proceeds through CO formed in an initial step. This is also the case for CO_2 hydrogenation on Cu/δ-MoC systems as commented below.

The energy profiles in Figure 8a indicate that, at 0 K, H_2O and CH_3OH desorption processes are likely to slow down the yield since desorption involves barriers of ∼0.8 eV. Furthermore, the energy difference between adsorbed reactants (CO_2* + 6H*) and the gas-phase desorbed products is around 2 eV indicating that, despite the fact that methanol synthesis is exothermic, the overall process is not favored. In order to gather information for the process under more realistic conditions, Figure 8b shows the Gibbs free energy profile for CO_2 hydrogenation to methanol on the clean δ-MoC(001) at the minimum and maximum temperatures (500 and 600 K) used in the experiments and also at different pressures (1 and 5 atm). Note that the Gibbs free energy barriers in the profiles in Figure 8b are identical to those reported in Figure 8a at 0 K. This is because calculated Gibbs free energy values neglect the entropic contributions from adsorbed species. Results in Figure S1 and Table S1 in the Supporting Information show that including these effects lead to variations on the energy barriers which are <0.1 eV. Consequently, the Gibbs free energy profiles

DOI: 10.1021/jacs.6b04529
J. Am. Chem. Soc. 2016, 138, 8269−8278

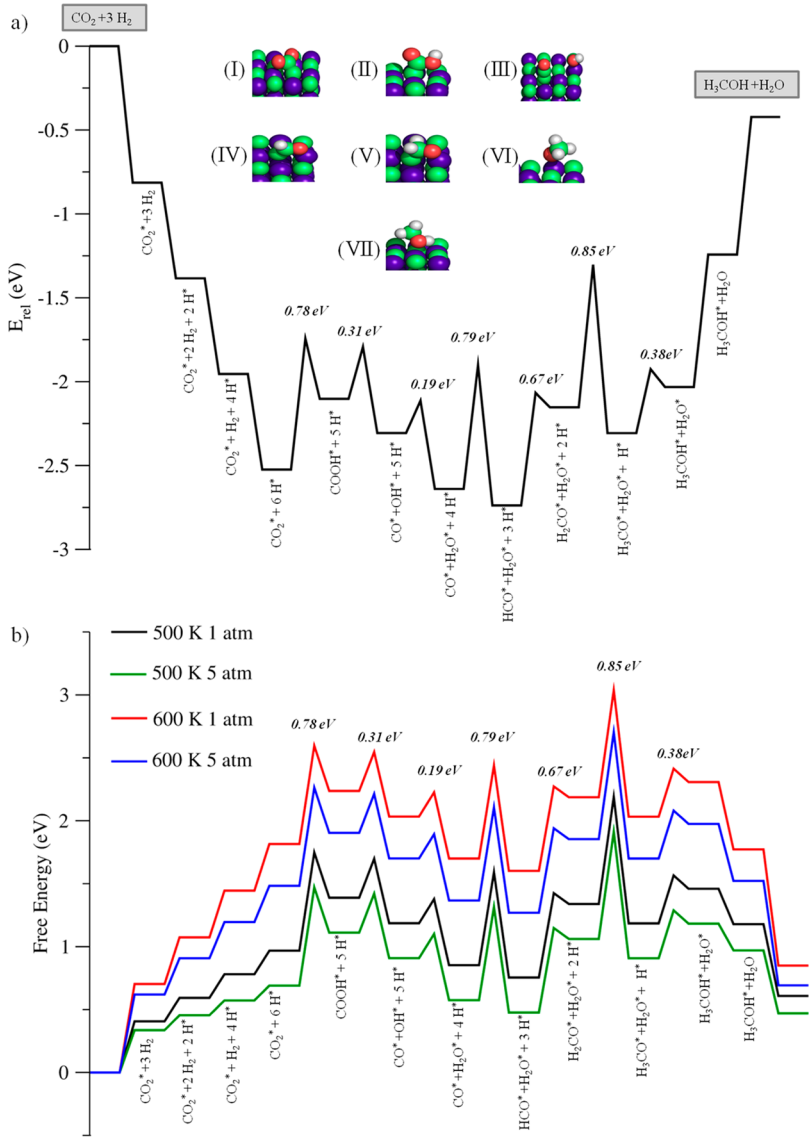

Figure 8. (a) Energy profile for the elementary steps involved in CO_2 hydrogenation on δ-MoC as predicted from DFT calculations on a δ-MoC(001) slab model. Sketches represents the adsorption of CO_2 (I), COOH (II), CO + OH (III), HCO (IV), H_2CO (V), H_3CO (VI), and CH_3OH (VII). (b) Gibbs free energy profiles of methanol synthesis at 500 and 600 K and at different pressures (1 and 5 atm).

for the Cu/δ-MoC system neglect the entropic contributions of adsorbed species. From the results in Figure 8, it is clear that CO_2 hydrogenation to methanol at 0 K is exergonic, while at 500 and 600 K the process becomes endergonic. However, the effect of temperature is crucial to favor H_2O and CH_3OH desorption. On the other hand, pressure effects affect adsorption and desorption thus facilitating methanol and water production.

To investigate the very large effect observed in the experiments when small Cu clusters are supported on δ-MoC, a computational model with a Cu_4 distorted rhombus structure supported on a δ-MoC(001) slab surface model was selected to represent the Cu/δ-MoC system. This choice is justified from the experimental evidence that the Cu clusters on the Cu/δ-MoC system are small, and from previous theoretical studies on several similar systems providing evidence that, in spite of some limitations due to the choice of the size of the supported clusters, these models describe the tendencies observed by experiments.[50−52,54] In fact, a recent study of the interaction of CO_2 with different Cu clusters of different size, including Cu_4, Cu_7, Cu_{10}, and a Cu monolayer, supported on β-Mo_2C shows that adsorption energies and energy barriers exhibit some dependence with size, but the main trends remain unchanged.[26] It is worth pointing out that previous work reported that for the supported Cu cluster a 3D pyramid structure is degenerate in energy with a 2D distorted rhombus.[38] However, the present DFT calculations show that upon CO_2 and CO adsorption on the supported Cu_4 pyramidal cluster triggers isomerization to rhombus geometry. Furthermore, the most stable structures of adsorbed CO_2 or CO also correspond to the supported Cu_4 rhombus. The interaction between the supported Cu_4 cluster and the δ-MoC support triggers some charge transfer from the metal to C surface atoms in such a way that the Cu cluster becomes slightly oxidized ($Cu^{\delta+}$ cluster). This is contrary to what has been found for Cu clusters deposited on Mo-terminated β-Mo_2C(001) surfaces where the Cu cluster is slightly reduced.[38] Furthermore, the DFT calculated adsorption energy for CO_2 on a Cu_4 cluster supported on δ-MoC(001) is ∼0.6 eV, whereas the CO_2 adsorption energy on the same Cu_4 cluster supported on β-

DOI: 10.1021/jacs.6b04529
J. Am. Chem. Soc. 2016, 138, 8269−8278

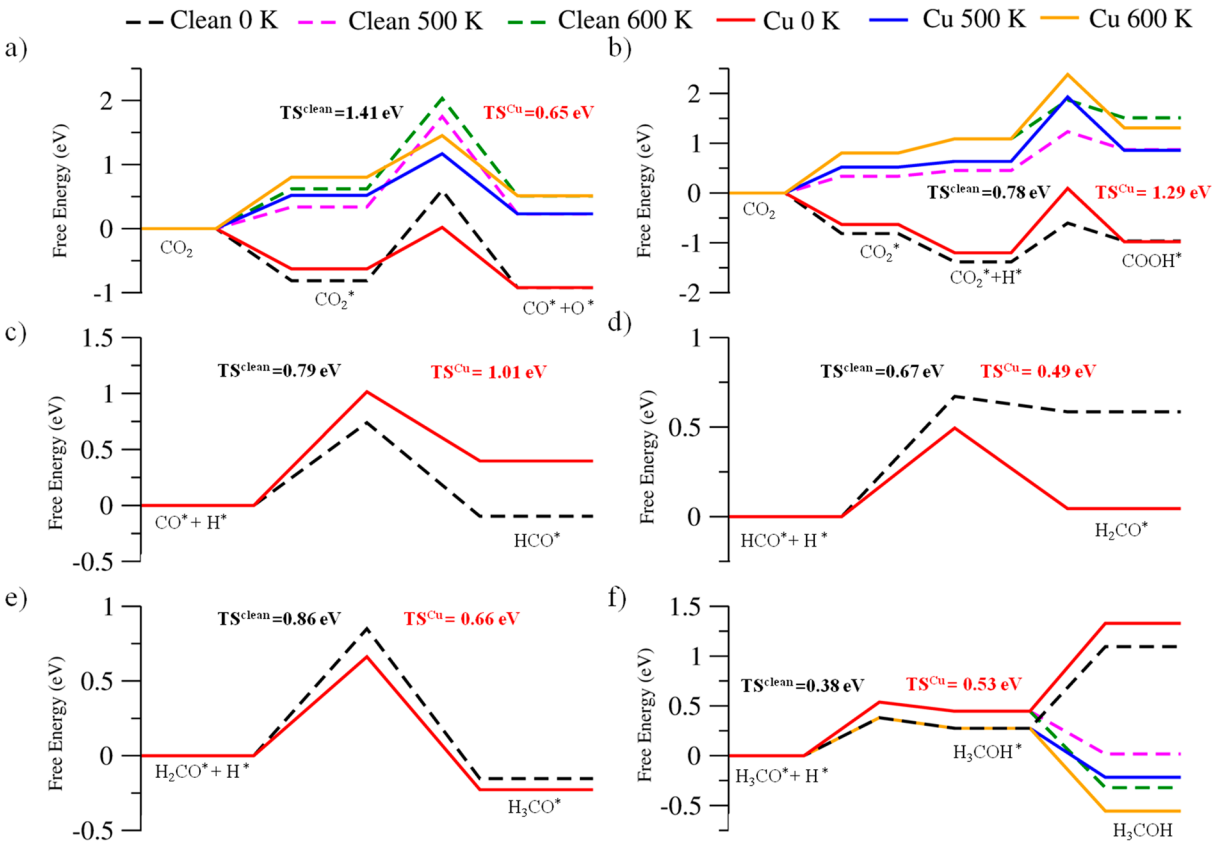

Figure 9. Calculated total energy (0 K) and Gibbs free energy (500 and 600 K at 5 atm) profiles for the most relevant elementary steps: (a) CO_2 dissociation, (b) CO_2 hydrogenation, (c) CO hydrogenation, (d) HCO hydrogenation, (e), H_2CO hydrogenation, and (f) methanol production as predicted from DFT calculations on a Cu_4/δ-MoC(001) model. Note that the effect of temperature and pressure only affect adsorption (a and b) and desorption (f) processes.

Mo_2C(001) is ~0.1 eV only.[38] Here, an impact of the metal/carbon ratio of the carbide on the properties of the supported system is clearly observed; it changes the chemical nature of the supported metal cluster opening a completely different reactivity. Note also that the interaction between CO_2 and the Cu_4 cluster supported on the δ-MoC(001) surface is ~0.6 eV, slightly smaller than on the clean surface (~0.8 eV). Nevertheless, this difference is small enough to have both types of sites occupied, especially at large coverage where most of the sites of the clean surface will be already occupied.

Let us now describe the essential results for CO_2 hydrogenation on the Cu_4 cluster supported on δ-MoC(001). Figure 9 compares total energy and Gibbs free energy profiles at 500 and 600 K and 5 atm for the relevant steps of CO_2 hydrogenation on the clean δ-MoC(001) and Cu_4/δ-MoC-(001). Again, the effect of temperature only is relevant for adsorption and desorption steps. Figure 9a shows that the presence of supported Cu clusters facilitates direct CO_2 dissociation to CO + O with a fairly small activation energy barrier (0.65 eV), a reaction that cannot occur in the clean surface δ-MoC(001) surfaces or on extended surfaces of copper such as Cu(111) or Cu(100).[37] Thus, on the Cu/δ-MoC system, there is synergy between the components of the catalyst, and CO production is easier (and likely faster) than on the clean surface, in agreement with the experimental observations (Figures 6 and 7). On the other hand, Figure 9b confirms the role of the supported Cu cluster in providing an alternative reaction pathway since here CO is produced from direct dissociation of CO_2 rather than from prior formation of the COOH intermediate and its subsequent dissociation which is the preferred pathway on the clean δ-MoC(001) surface. It is worth pointing out that on the supported cluster, at variance of the clean surface, direct CO_2 hydrogenation to formate (HCOO) is likely to occur. This is not unexpected since formate is typically observed on CO_2 hydrogenation using Cu as catalysts.[60−62] Nevertheless, formate decomposition to the HCO intermediate is very unlikely since it is endothermic by 1.4 eV and HCOO hydrogenation toward formic acid or dioxymethylene (H_2COO), as previous step of H_2CO formation[26,56] presents large energy barriers; 1.40 eV to H_2COO formation. Clearly, reaction pathways via formate can be discarded, and this species will at most behave as an spectator perhaps poisoning the surface.

On the Cu_4/δ-MoC(001) model system, following the first crucial step involving CO_2 dissociation, which represents the main difference with respect to the clean δ-MoC(001) surface, the overall computational study shows that the reaction proceeds at the clean surface via the HCO intermediate (Figure 9c). It is worth pointing out that, while CO is produced mostly at the supported cluster and also partly at the clean surface, some of the further hydrogenation steps are facilitated by the presence of the support. In fact, compared to the clean surface, CO hydrogenation at Cu and Cu−Mo interface sites entails a higher energy barrier (~0.95 eV). Note that even if a direct comparison is not possible, this energy barrier probably would increase the apparent activation energy, which is not

DOI: 10.1021/jacs.6b04529
J. Am. Chem. Soc. 2016, 138, 8269−8278

observed on the experiments. Therefore, one must accept that the CO produced on Cu_4/MoC(001) would diffuse to clean surface region. Calculations show that this is indeed thermodynamically favorable since adsorption at sites of the clean surface (E_{ads} = −1.91 eV) is preferred to adsorption at Cu sites (E_{ads} = −1.15 eV), and the calculated diffusion energy barriers from the supported cluster to the surface clean region are much smaller. Besides its relevant role on triggering CO_2 dissociation, Cu_4 and the Cu-MoC interface sites also play a crucial role on several hydrogenations steps. For instance, the energy barrier of H_2CO formation from HCO is reduced from 0.67 eV on the bare surface to 0.49 eV (Figure 9d), and subsequent hydrogenation to H_3CO is also more favorable at Cu sites; the energy barrier decreases from 0.85 eV on the bare surface to 0.66 eV at Cu sites of the supported cluster (Figure 9e). The profiles for last hydrogenation to methanol are also displayed on Figure 9f and imply an energy barrier higher than on the bare surface (0.53 eV). This is, however, lower than the energy barriers for the previous steps, and furthermore, methanol could also be formed on the clean region. Finally, note that temperature and pressure effects affect mainly the desorption step which becomes more favorable. Overall, as a result of metal-support interactions and a synergy at the metal-carbide interface, Cu/δ-MoC is an excellent catalyst for the activation of CO_2.

CONCLUSIONS

A new set of Au/δ-MoC and Cu/δ-MoC catalysts exhibits high activity, selectivity, and stability for the transformation of CO_2 to CO and methanol, without the generation of methane as a side product. Unique interactions with the metal carbide support enhance the chemical reactivity of Au and Cu, making the Au/δ-MoC and Cu/δ-MoC catalysts more active than a model for an industrial Cu/ZnO catalyst or the isolated metals.

A comparison of the behavior of Au and Cu aggregates supported on TiC, δ-MoC and β-Mo_2C shows that the metal/carbon ratio in the carbide plays a key role in defining the reactivity of the supported metals and in preventing catalyst deactivation by the formation of an oxycarbide.

Theoretical calculations based on DFT provide several clues for the origin of the high activity and selectivity observed for Cu/δ-MoC in experimental tests. The calculations indicate that the Cu/δ-MoC system works as a bifunctional catalyst, where the supported Cu clusters readily dissociate CO_2 into CO and O, whereas both the clean regions of the δ-MoC substrate and the supported clusters catalyze the main hydrogenation steps toward methanol and water. In this way, the supported Cu clusters open a new route to CO without requiring the assistance of COOH intermediate, as in a clean δ-MoC(001) surface. In this sense, the use of Cu/δ-MoC catalysts for CO_2 conversion is encouraging with possible applications in technical or industrial operations.

ASSOCIATED CONTENT

Supporting Information

The Supporting Information is available free of charge on the ACS Publications website at DOI: 10.1021/jacs.6b04529.

Gibbs free energy profiles for CO_2 hydrogenation to methanol on clean δ-MoC(001) at 500 and 600 K and at 1 and 5 atm including or not the entropic contributions of adsorbed species and Gibbs free energy barriers for CO_2 hydrogenation to methanol on clean δ-MoC(001) at different conditions including the entropic contribution of adsorbed species (PDF)

AUTHOR INFORMATION

Corresponding Authors

*francesc.illas@ub.edu

*rodrigez@bnl.gov

Notes

The authors declare no competing financial interest.

ACKNOWLEDGMENTS

This manuscript has been authored by employees of Brookhaven Science Associates, LLC under Contract No. DE-SC0012704 with the U.S. Department of Energy. The research carried out at the Universitat de Barcelona was supported by the Spanish MINECO/FEDER grant CTQ2015-64618-R and, in part, by Generalitat de Catalunya (grants 2014SGR97 and XRQTC) and from the NOMAD Center of Excellence project; the latter project has received funding from the European Union's Horizon 2020 research and innovation programme under grant agreement no. 676580. S.P.P. acknowledges financial support from Spanish MEC predoctoral grant associated with CTQ2012-30751. F.V. thanks the MINECO for a postdoctoral Ramón y Cajal (RyC) research contract (RYC-2012-10129), and F.I. acknowledges additional support from the 2015 ICREA Academia Award for Excellence in University Research. Computational time at the MARENOSTRUM supercomputer has been provided by the Barcelona Supercomputing Centre (BSC) through a grant from Red Española de Supercomputación (RES).

REFERENCES

(1) Lim, X. *Nature* **2015**, *526*, 628.

(2) Intergovernmental Panel on Climate Change. *Climate Change 2013, The Physical Science Basis*, 1st ed.; Cambridge University Press: Cambridge, U.K., 2014.

(3) Preti, D.; Resta, C.; Squarcialupi, S.; Fachinetti, G. *Angew. Chem., Int. Ed.* **2011**, *50*, 12551.

(4) Aresta, M. *Carbon Dioxide as Chemical Feedstock*; Wiley-VCH, New York, 2010.

(5) Porosoff, M. D.; Yang, X.; Chen, J. G. *Energy Environ. Sci.* **2016**, *9*, 62.

(6) Wang, S.; Lu, G. Q.; Millar, G. J. *Energy Fuels* **1996**, *10*, 896.

(7) Caballero, A.; Perez, P. J. *Chem. Soc. Rev.* **2013**, *42*, 8809.

(8) Liu, X. M.; Lu, G. Q.; Yan, Z. F.; Beltramini, J. *Ind. Eng. Chem. Res.* **2003**, *42*, 6518.

(9) Xiaoding, X.; Moulijn, J. A. *Energy Fuels* **1996**, *10*, 305.

(10) Martin, O.; Martín, A. J.; Mondelli, C.; Mitchell, S.; Segawa, T. F.; Hauert, R.; Droully, C.; Curulla-Ferré, D.; Pérez-Ramírez, J. *Angew. Chem., Int. Ed.* **2016**, *55*, 6261.

(11) Kondratenko, E. V.; Mul, G.; Baltrusaitis, J.; Larrazábal, G. O.; Pérez-Ramírez, J. *Energy Environ. Sci.* **2013**, *6*, 3112.

(12) Thomas, J. M.; Thomas, W. J. *Principles and Practice of Heterogeneous Catalysis*; Wiley-VCH, New York, 1996.

(13) Levy, R. B.; Boudart, M. *Science* **1973**, *181*, 547.

(14) Claridge, J. B.; York, A. P. E.; Brungs, A. J.; Marquez-Alvarez, C.; Sloan, J.; Tsang, S. C.; Green, M. L. H. *J. Catal.* **1998**, *180*, 85.

(15) Didziulis, S. V.; Butcher, K. D. *Coord. Chem. Rev.* **2013**, *257*, 93.

(16) Koos, A.; Solymosi, F. *Catal. Lett.* **2010**, *138*, 23.

(17) Posada-Perez, S.; Viñes, F.; Ramirez, P. J.; Vidal, A. B.; Rodriguez, J. A.; Illas, F. *Phys. Chem. Chem. Phys.* **2014**, *16*, 14912.

(18) Oshikawa, K.; Nagai, M.; Omi, S. *J. Phys. Chem. B* **2001**, *105*, 9124.

(19) Viñes, F.; Liu, P.; Rodriguez, J. A.; Illas, F. *J. Catal.* **2008**, *260*, 103.

DOI: 10.1021/jacs.6b04529
J. Am. Chem. Soc. 2016, 138, 8269−8278

(20) Oyama, S. T. *Catal. Today* **1992**, *15*, 179.
(21) Barthos, R.; Solymosi, F. *J. Catal.* **2007**, *249*, 289.
(22) Li, L.; Sholl, D. S. *ACS Catal.* **2015**, *5*, 5174.
(23) Posada-Pérez, S.; Viñes, F.; Rodriguez, J. A.; Illas, F. *Top. Catal.* **2015**, *58*, 159.
(24) Viñes, F.; Vojvodic, A.; Abild-Pedersen, F.; Illas, F. *J. Phys. Chem. C* **2013**, *117*, 4168.
(25) Hwu, H. H.; Chen, J. G. *Chem. Rev.* **2005**, *105*, 185.
(26) Posada-Pérez, S.; Ramirez, P. J.; Gutierrez, R. A.; Stacchiola, D. J.; Viñes, F.; Liu, P.; Illas, F.; Rodriguez, J. A. *Catal. Sci. Technol.* DOI: 10.1039/c5cy02143j.
(27) Kunkel, C.; Viñes, F.; Illas, F. *Energy Environ. Sci.* **2016**, *9*, 141.
(28) Rodriguez, J. A.; Evans, J.; Feria, L.; Vidal, A. B.; Liu, P.; Nakamura, K.; Illas, F. *J. Catal.* **2013**, *307*, 162.
(29) Rodriguez, J. A.; Illas, F. *Phys. Chem. Chem. Phys.* **2012**, *14*, 427.
(30) Ono, L. K.; Roldan-Cuenya, B. *Catal. Lett.* **2007**, *113*, 86.
(31) Porosoff, M. D.; Yang, X.; Boscoboinik, J. A.; Chen, J. G. *Angew. Chem., Int. Ed.* **2014**, *53*, 6705.
(32) Liu, P.; Rodriguez, J. A. *J. Phys. Chem. B* **2006**, *110*, 19418.
(33) Vidal, A. B.; Feria, L.; Evans, J.; Takahashi, Y.; Liu, P.; Nakamura, K.; Illas, F.; Rodriguez, J. A. *J. Phys. Chem. Lett.* **2012**, *3*, 2275.
(34) Liu, P.; Rodriguez, J. A.; Asakura, T.; Gomes, J.; Nakamura, K. *J. Phys. Chem. B* **2005**, *109*, 4575.
(35) Chen, J. G. *Chem. Rev.* **1996**, *96*, 1477.
(36) Yoshihara, J.; Campbell, C. T. *J. Catal.* **1996**, *161*, 776.
(37) Yang, Y.; Evans, J.; Rodriguez, J. A.; White, M. G.; Liu, P. *Phys. Chem. Chem. Phys.* **2010**, *12*, 9909.
(38) Posada-Pérez, S.; Viñes, F.; Rodriguez, J. A.; Illas, F. *J. Chem. Phys.* **2015**, *143*, 114704.
(39) Politi, J. R. d. S.; Viñes, F.; Rodriguez, J. A.; Illas, F. *Phys. Chem. Chem. Phys.* **2013**, *15*, 12617.
(40) Perdew, J. P.; Burke, K.; Ernzerhof, M. *Phys. Rev. Lett.* **1996**, *77*, 3865.
(41) Kresse, G.; Furthmuüller, J. *Phys. Rev. B: Condens. Matter Mater. Phys.* **1996**, *54*, 11169.
(42) Blöchl, P. E. *Phys. Rev. B: Condens. Matter Mater. Phys.* **1994**, *50*, 17953.
(43) Kresse, G.; Joubert, D. *Phys. Rev. B: Condens. Matter Mater. Phys.* **1999**, *59*, 1758.
(44) Monkhorst, H. J.; Pack, J. D. *Phys. Rev. B* **1976**, *13*, 5188.
(45) Henkelman, G.; Jonsson, H. *J. Chem. Phys.* **1999**, *111*, 7010.
(46) Nørskov, J. K.; Studt, F.; Abild-Pedersen, F.; Bligaard, T. *Fundamental Concepts in Heterogeneous Catalysis*; Wiley, Hoboken, NJ, 2014.
(47) Liu, P.; Rodriguez, J. A. *J. Chem. Phys.* **2004**, *120*, 5414.
(48) Xu, W.; Ramirez, P. J.; Stacchiola, D.; Rodriguez, J. A. *Catal. Lett.* **2014**, *144*, 1418.
(49) Wang, T.; Li, Y. W.; Wang, J.; Beller, M.; Jiao, H. *J. Phys. Chem. C* **2014**, *118*, 3162.
(50) Rodriguez, J. A.; Liu, P.; Viñes, F.; Illas, F.; Takahashi, Y.; Nakamura, K. *Angew. Chem., Int. Ed.* **2008**, *47*, 6685.
(51) Rodriguez, J. A.; Liu, P.; Takahashi, Y.; Nakamura, K.; Viñes, F.; Illas, F. *J. Am. Chem. Soc.* **2009**, *131*, 8595.
(52) Feria, L.; Rodriguez, J. A.; Jirsak, T.; Illas, F. *J. Catal.* **2011**, *279*, 352.
(53) Rodriguez, J. A.; Feria, L.; Jirsak, T.; Takahashi, Y.; Nakamura, K.; Illas, F. *J. Am. Chem. Soc.* **2010**, *132*, 3177.
(54) Rodriguez, J. A.; Ramirez, P. J.; Asara, G. G.; Viñes, F.; Evans, J.; Liu, P.; Ricart, J. M.; Illas, F. *Angew. Chem., Int. Ed.* **2014**, *53*, 11270.
(55) Tominaga, H.; Aoki, Y.; Nagai, M. *Appl. Catal., A* **2012**, *423*−*424*, 192.
(56) Grabow, L. C.; Mavrikakis, M. *ACS Catal.* **2011**, *1*, 365.
(57) Wang, J.; Kawazoe, Y.; Sun, Q.; Chan, S.; Su, H. *Surf. Sci.* **2016**, *645*, 30.
(58) Grabow, L. C.; Gokhale, A. A.; Evans, S. T.; Dumesic, J. A.; Mavrikakis, M. *J. Phys. Chem. C* **2008**, *112*, 4608.
(59) Prats, H.; Álvarez, L.; Illas, F.; Sayós, R. *J. Catal.* **2016**, *333*, 217.
(60) Liu, C.; Yang, B.; Tyo, E.; Seifert, S.; De Bartolo, J.; von Issendorff, B.; Zapol, P.; Vajda, S.; Curtiss, L. A. *J. Am. Chem. Soc.* **2015**, *137*, 8676.
(61) Studt, F.; Behrens, M.; Kunkes, E. L.; Thomas, N.; Zander, S.; Tarasov, A.; Schumann, J.; Frei, E.; Varley, J. B.; Abil-Pedersen, F.; Norskov, J. K.; Schlogl, R. *ChemCatChem* **2015**, *7*, 1105.
(62) Kim, Y.; Trung, T. S. B.; Yang, S.; Kim, S.; Lee, H. *ACS Catal.* **2016**, *6*, 1037.

DOI: 10.1021/jacs.6b04529
J. Am. Chem. Soc. 2016, 138, 8269−8278